Tailoring dielectric properties of ferroelectric-dielectric multilayers

M. T. Kesim, M. W. Cole, J. Zhang, I. B. Misirlioglu, and S. P. Alpay

Citation: Applied Physics Letters **104**, 022901 (2014); doi: 10.1063/1.4861716
View online: http://dx.doi.org/10.1063/1.4861716
View Table of Contents: http://scitation.aip.org/content/aip/journal/apl/104/2?ver=pdfcov
Published by the AIP Publishing

Tailoring dielectric properties of ferroelectric-dielectric multilayers

M. T. Kesim,[1] M. W. Cole,[2] J. Zhang,[1] I. B. Misirlioglu,[3] and S. P. Alpay[1,4,a)]
[1]*Department of Materials Science and Engineering and Institute of Materials Science, University of Connecticut, Storrs, Connecticut 06269, USA*
[2]*U.S. Army Research Laboratory, Weapons and Materials Research Directorate, Aberdeen Proving Ground, Maryland 21005, USA*
[3]*Faculty of Engineering and Natural Sciences, Sabancı University, Orhanlı/Tuzla, 34956 Istanbul, Turkey*
[4]*Department of Physics, University of Connecticut, Storrs, Connecticut 06269, USA*

(Received 10 December 2013; accepted 27 December 2013; published online 13 January 2014)

We develop a nonlinear thermodynamic model for multilayer ferroelectric heterostructures that takes into account electrostatic and electromechanical interactions between layers. We concentrate on the effect of relative layer fractions and in-plane thermal stresses on dielectric properties of $Ba_{0.6}Sr_{0.4}TiO_3$-, $BaTiO_3$-, and $PbZr_{0.2}Ti_{0.8}O_3$ (PZT)-$SrTiO_3$ (STO) multilayers on Si and *c*-sapphire. We show that dielectric properties of such multilayers can be significantly enhanced by tailoring the growth/processing temperature and the STO layer fraction. Our computations show that large tunabilities (~90% at 400 kV/cm) are possible in carefully designed barium strontium titanate-STO and PZT-STO even on Si for which there exist substantially large in-plane strains. © *2014 AIP Publishing LLC*. [http://dx.doi.org/10.1063/1.4861716]

Non-linear dielectric materials have been considered as voltage-controlled frequency-agile elements in tunable microwave and millimeter wave devices such as capacitors, phase shifters, resonators, and oscillators.[1] Ferroelectrics (FEs) such as barium strontium titanate (BST, $Ba_{1-x}Sr_xTiO_3$) have emerged as leading candidates for such applications due to their highly non-linear dielectric response to an applied electric field, especially in the vicinity of the paraelectric (PE)-to-FE phase transformation temperature T_C.[2–5] In BST, T_C can be controlled via the composition. For example, bulk T_C of BST 70/30 ($Ba_{0.70}Sr_{0.30}TiO_3$) is just below room temperature (~15 °C).[2] As such, FEs and, in particular, BST, have been investigated for over a decade as potential candidates in tunable components in telecommunications since the utilization of DC fields for tuning improves the response speed and the power consumption of the device.[6,7] The major challenge in designing materials systems for tunable devices is the simultaneous requirement of high tunability (>40%) over a large temperature interval (−20 °C to +85 °C), and low dielectric losses (between 3.0 and 4.0 dB in operational bandwidths ranging from several hundred MHz over 30 GHz).[8–10] It is usually desired in telecommunication applications that FEs are in a PE state to eliminate losses resulting from polarization switching-induced hysteresis, domain wall contributions, and piezoelectric transformations at microwave frequencies.[10,11] Nevertheless, there are reports of acceptable dielectric properties in the FE state as well.[10–13]

Significant efforts have been devoted to maintain high dielectric tunability and to decrease dielectric losses through doping and by constructing a variety of composite structures consisting of FE/PE active materials and low-loss and low leakage oxides and polymers.[11,14] Among such composites, carefully designed FE/PE/dielectric multilayers, superlattices, and compositionally graded structures display improved dielectric properties than their bulk and single-crystal counterparts due to electrostatic and electromechanical interlayer interactions. Such materials systems have been shown to be promising candidates in microwave telecommunication applications.[15–20]

In this letter, the dielectric properties of FE heterostructures with PE buffer layers on IC-compatible Si and *c*-sapphire substrates are investigated using a non-linear thermodynamic model that takes into account the thermal stresses that develop during cooling from the growth/processing temperature (T_G) and the electrostatic coupling between the layers that make up the multilayer construct. We note that the rationale for this study originates from theoretical studies that reveal the existence of a dielectric anomaly in coupled FE-PE bilayers at a critical PE layer fraction resulting from electrostatic interactions that suppress ferroelectricity.[16,21] This is considered to be analogous to the dielectric maxima observed near T_C in monolithic FEs. This concept has been employed to improve dielectric tunability in microwave and millimeter wave tunable telecommunication devices.[16] The use of a PE layer as a buffer layer in device configuration is also attractive because experimental results show clear improvements in leakage characteristics. For example, ~200 nm thick Mg-doped BST-$SrTiO_3$ (STO) bilayer heterostructures on metallized *c*-sapphire substrates display enhanced dielectric properties with low losses (~0.02) and leakage currents (7×10^{-9} A/cm^2) when compared to Mg-doped BST films without buffer layers. It was reported that decreasing the thickness of the PE layer (i.e., the layer fraction) from 41 to 19 nm leads to an improvement in the (relative) dielectric constant ε_R by nearly 35%.[22] It has also been shown that the critical heterostructure composition/configuration corresponding to a dielectric anomaly is quite sensitive to changes in the amount of misfit and thermal stresses.[23–25] It is, therefore, of great scientific and technological interest to investigate the effect of strains in multilayers with different multilayer-substrate configurations to tailor desired dielectric properties in detail.

a)Author to whom correspondence should be addressed. Electronic mail: p.alpay@ims.uconn.edu

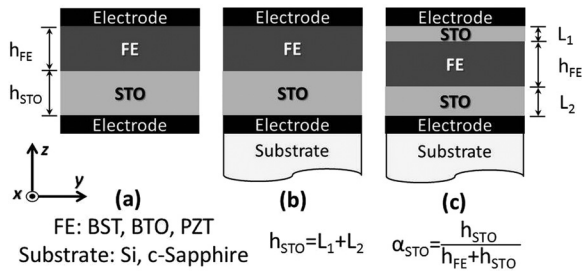

FIG. 1. (a) Freestanding (unconstrained) and (b) clamped FE-STO bilayer sandwiched between top and bottom metallic electrodes on a thick substrate, (c) clamped STO-FE-STO trilayer on a substrate.

We consider here a [001]-oriented polycrystalline multilayer composed of a monodomain $Ba_{0.6}Sr_{0.4}TiO_3$ (BST 60/40), $BaTiO_3$ (BTO), or $PbZr_{0.2}Ti_{0.8}O_3$ (PZT 20/80) layer and a STO buffer layer (Fig. 1(a)) on a thick Si or *c*-sapphire substrate (Figs. 1(b) and 1(c)). We assume the multilayer is processed at a temperature T_G before cooling to room temperature (RT = 25 °C). In a multilayer heterostructure, the in-plane strain between layer *i* and the much thicker substrate $u_{T,i}$ due to the thermal stresses is given by

$$u_{T,i}(T_G) = \int_{T}^{T_G} (\alpha_{F,i} - \alpha_S) dT, \tag{1}$$

where $\alpha_{F,i}$ and α_S are the in-plane coefficients of thermal expansion (CTE) of the layer *i* and the substrate, respectively. The total free energy density of such a system can be expressed as[16]

$$G = (1-\alpha)\cdot G_1(P_1, T, u_{T,1}, E) + \alpha \cdot G_2(P_2, T, u_{T,2}, E) + \frac{1}{2}\alpha(1-\alpha)\frac{1}{\varepsilon_0}(P_1 - P_2)^2 + \frac{G_S}{h}. \tag{2}$$

The details of the derivation of the above relation are given elsewhere.[16] Here, $\alpha = \alpha_{STO} = h_{STO}/(h_{FE} + h_{STO})$ is the relative thickness (layer fraction) of the STO layer, where h_{FE} and h_{STO} are the thicknesses of the FE and STO layers, respectively, and $h = h_{FE} + h_{STO}$ is the total thickness of the multilayer. We note here that the last term in total free energy given by Eq. (2) is the interfacial energy between the layers and it can be neglected for sufficiently thick multilayers with thicknesses larger than the correlation length of ferroelectricity.[26] In Eq. (2), P_i is the polarization of layer *i* normal to the interlayer interface, and *E* is an applied electrical field parallel to the polarization. The third term in the above free energy functional expresses the electrostatic coupling between the layers. G_1 and G_2 are the uncoupled free energies of the FE and STO layers, respectively, given by

$$G_i(P_i, T, u_{T,i}, E) = G_{0,i} + \tilde{a}_i P_i^2 + \tilde{b}_i P_i^4 + c_i P_i^6 + \frac{u_{T,i}^2}{S_{11} + S_{12}} - EP_i, \tag{3}$$

with renormalized dielectric coefficients $\tilde{a}_i$ and $\tilde{b}_i$

$$\tilde{a}_i = a_i - \frac{2Q_{12,i}}{S_{11,i} + S_{12,i}} u_{T,i}, \quad \tilde{b}_i = b_i + \frac{Q_{12,i}^2}{S_{11,i} + S_{12,i}}, \tag{4}$$

where a_i, b_i, and c_i are the bulk dielectric stiffness coefficients. The quadratic coefficient a_i is given by the Curie-Weiss Law, $a_i = (T - T_C)/2\varepsilon_0 C$, where ε_0 is the permittivity of free space and *C* is the Curie-Weiss constant. $Q_{ij,i}$ and $S_{ij,i}$ are the electrostrictive coefficients and the elastic compliances at constant polarization of layer *i*. The dielectric stiffness and thermal expansion coefficients were obtained from the literature.[27–30]

The equilibrium polarizations ${P_1}^0$ and ${P_2}^0$ along *z* in the coupled layer are provided by the equations of state $\partial G/\partial P_1 = 0$ and $\partial G/\partial P_2 = 0$ such that

$$\left[2\tilde{a}_1 + \frac{\alpha(1-\alpha)}{\varepsilon_0}\right]\cdot P_1 + 4\tilde{b}_1 P_1^3 + 6c_1 P_1^5 - \frac{\alpha(1-\alpha)}{\varepsilon_0} P_2 = 0, \tag{5}$$

$$\left[2\tilde{a}_2 + \frac{\alpha(1-\alpha)}{\varepsilon_0}\right]\cdot P_2 + 4\tilde{b}_2 P_2^3 + 6c_2 P_2^5 - \frac{\alpha(1-\alpha)}{\varepsilon_0} P_1 = 0. \tag{6}$$

The average dielectric response of the multilayer is

$$\langle \varepsilon_R \rangle = \frac{1}{\varepsilon_0}\frac{d\langle P\rangle}{dE} = \frac{1}{\varepsilon_0}\left[(1-\alpha)\frac{dP_1^0}{dE} + \alpha\frac{dP_2^0}{dE}\right], \tag{7}$$

where $\langle P\rangle = (1-\alpha){P_1}^0 + \alpha {P_2}^0$ is the average polarization.

A freestanding multilayer configuration in Fig. 1(a) is chosen as the reference state to understand the role of two-dimensional clamping and thermal stresses on the dielectric properties more clearly, see Eqs. (2)–(6). Figs. 2 and 3 plot the small signal ε_R of the multilayers with BTO and BST as the FE layers, respectively, on Si and *c*-sapphire. As shown in Fig. 2, RT ε_R of unconstrained (bulk) BST is over 2400, whereas the dielectric response of films with $\alpha_{STO} = 0.1$ on Si and *c*-sapphire for $T_G = 550$ °C are 554 and 683, respectively. This is expected since thermally induced in-plane tensile strains and the interlayer coupling both decrease T_C of the FE in such a multilayer configuration. Therefore, such electrical and mechanical boundary conditions are particularly detrimental for the dielectric response if the FE is already in the PE state as it is the case for BST 60/40 at RT, Fig. 2. As T_C moves far below RT in the clamped, in-plane strained condition, an appreciable polarization change cannot be induced upon the application of a biasing field. This is

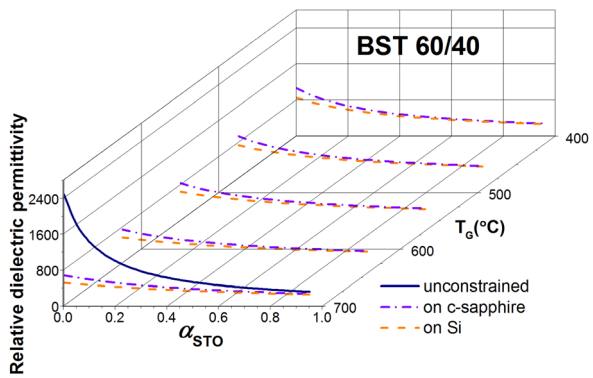

FIG. 2. Small signal mean relative dielectric permittivity of polycrystalline BST 60/40-STO multilayer as functions of T_G and STO layer fraction on Si and *c*-sapphire substrates.

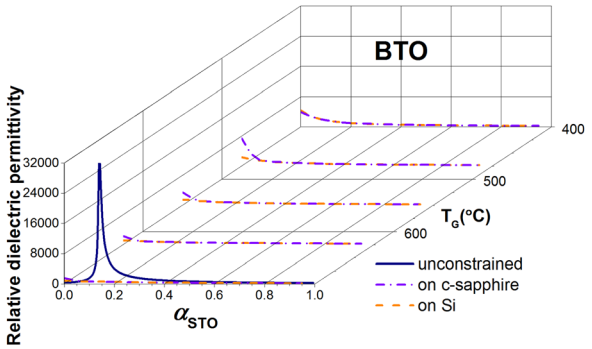

FIG. 3. Small signal mean relative dielectric permittivity of polycrystalline BTO-STO multilayer as functions of T_G and STO layer fraction on Si and *c*-sapphire substrates.

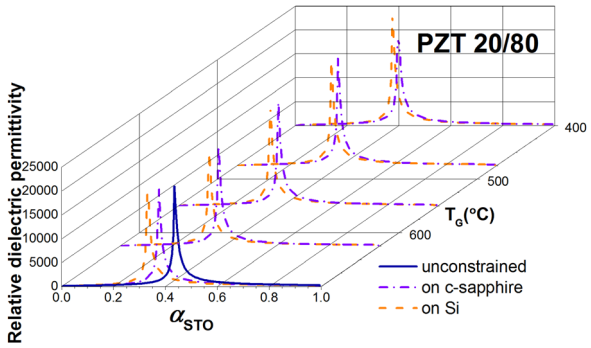

FIG. 4. Small signal mean relative dielectric permittivity of polycrystalline PZT 20/80-STO multilayer as functions of T_G and STO layer fraction on Si and *c*-sapphire substrates.

especially critical for films processed at higher T_Gs, since the dielectric maximum, corresponding to the FE-PE phase transition, is shifted to lower temperatures. This is clearly observed in Fig. 2; a lower T_G results in higher ε_R values on both substrates. For example, if T_G could be decreased from 700 °C to 550 °C for BST on Si with $\alpha_{STO} = 0.1$, we expect that there will be approximately 24% enhancement in ε_R. Fig. 2 also shows that employing STO buffer layers in configurations illustrated in Fig. 1 reduces ε_R of the heterostructure with increasing α_{STO} since ε_R of STO is lower than BST. This decrease is non-linear, clearly highlighting the role of electrostatic coupling between BST 60/40 and STO. For the dielectric properties of BTO monolayers ($\alpha_{STO} = 0$), the choice of the substrate and T_G becomes more critical (Fig. 3). This is entirely due to the shift of the bulk T_C (120 °C (Ref. 31)) to lower temperatures. As an example, changing T_G from 625 °C to 475 °C for BTO on *c*-sapphire results in a 51 °C difference in their transition temperatures ($T_{C,625\,°C} = -46$ °C and $T_{C,475\,°C} = +5$ °C). Very high dielectric permittivity values can be obtained near the instability from BTO on *c*-sapphire at a critical $T_G = 475$ °C. Fig. 3 also shows that the dielectric anomaly in unconstrained but electrostatically coupled heterostructures disappears if such bilayers are on *c*-sapphire and Si due to the in-plane tensile thermal strains and the clamping effect of the substrate. Even at a low T_G such as 400 °C, the magnitude of the thermal strains is sufficient to promote a PE state at RT in the BTO layer on both Si and *c*-sapphire. Therefore, BTO-STO displays similar behavior to BST 60/40-STO multilayers in that overall ε_R deteriorates as with increasing α_{STO} as a result of the shift of T_C with respect to RT.

Fig. 4 plots RT small signal ε_R of PZT 20/80-STO multilayers on Si and *c*-sapphire as functions of T_G and the STO layer fraction. PZT was chosen as the last example in our analysis because its bulk, unconstrained T_C (459 °C (Ref. 29)) is substantially higher than that of BST 60/40 and BTO. The dielectric response of PZT 20/80 as a function of α_{STO} in both unconstrained and thin film configurations exhibits a similar trend for all T_G. When PZT is electrostatically and electromechanically coupled with STO, there is a λ-type anomaly in the dielectric response as observed in Fig. 4 where the critical α_{STO} varies between 0.2 and 0.4 depending on T_G. The monotonic decrease in ε_R as a function of α_{STO} shown in Figs. 2 and 3 for BST and BTO on Si and *c*-sapphire is not observed for PZT 20/80 on the same substrates. This means that it is feasible to obtain a very strong dielectric response in PZT-STO heterostructures near the instability at a critical α_{STO} that depends on the processing temperature T_G.

The influence of an applied bias along the *z*-direction on the small signal ε_R and dielectric tunability ($\eta = (1 - \varepsilon_{R,E}/\varepsilon_{R,E=0}) \times 100$, at $E = 400$ kV/cm) of BTO- ($\alpha_{STO} = 0.1$), BST 60/40- ($\alpha_{STO} = 0.1$), and PZT 20/80-STO ($\alpha_{STO} = 0.35$ and 0.40) multilayers on Si and *c*-sapphire for $T_G = 700$ °C is illustrated in Figs. 5 and 6, respectively. The justification for the selection of α_{STO} follows from Figs. 2–4. High tunabilities over 60% and 90% at 400 kV/cm can be realized in BTO- ($\alpha_{STO} = 0.1$) and PZT-STO ($\alpha_{STO} = 0.35$ and 0.4) multilayers, respectively, at $T_G = 700$ °C, which is a typical processing temperature for perovskites.

We note that introducing STO buffer layers to improve loss and leakage characteristics of BST films decreases their ε_R, as it has been observed experimentally.[23] Therefore, BST

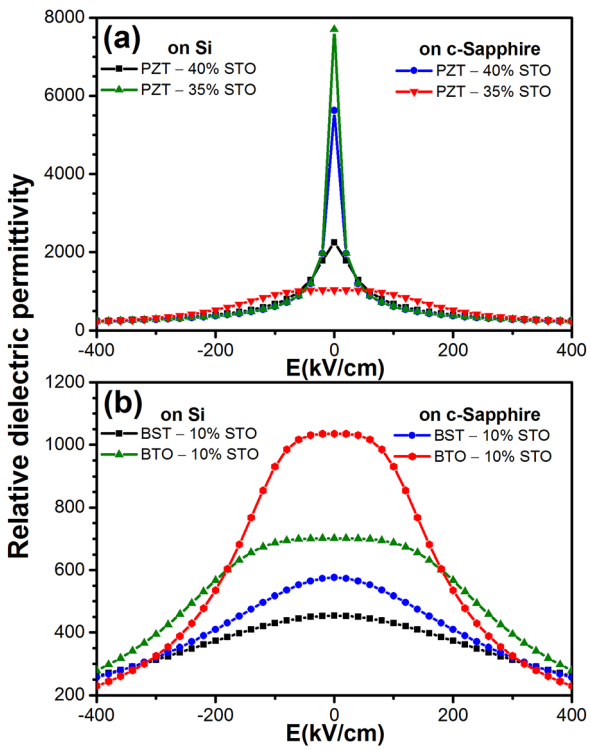

FIG. 5. Small signal mean relative dielectric permittivity of (a) PZT 20/80 (for $\alpha_{STO} = 0.35$ and 0.4) and (b) BTO (for $\alpha_{STO} = 0.1$), BST 60/40 (for $\alpha_{STO} = 0.1$) on Si and *c*-sapphire for $T_G = 700$ °C.

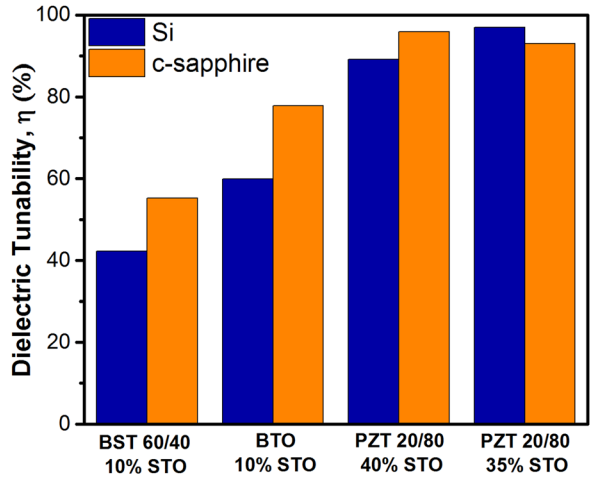

FIG. 6. Dielectric tunability of BST 60/40 (for $\alpha_{STO} = 0.1$), BTO (for $\alpha_{STO} = 0.1$), and PZT 20/80 (for $\alpha_{STO} = 0.35$ and 0.4) on Si and *c*-sapphire at $E = 400$ kV/cm for $T_G = 700\,^{\circ}$C.

or BTO multilayer configurations with thin PE buffer layers on IC compatible substrates (Fig. 1(b) or 1(c)) should be understood as a compromise between loss and leakage and dielectric permittivity and tunability. On the other hand, PZT-based FE-PE heterostructures offer an opportunity to tailor desired dielectric response near the instability by varying α_{STO} at a given T_G. Although such an enhanced dielectric response is extremely beneficial, as in the case of the BST and BTO multilayer configurations, to be useful in practical tunable device configurations the exceptionally high dielectric response of the PZT-based heterostructure must also be accompanied by low dielectric loss, low leakage current characteristics, and high breakdown field. Nevertheless, the fact the ferroelectric instability can be tuned as a function of PE buffer layer thickness and process temperatures opens a new region of materials process parameter space to be explored and exploited for voltage-controlled frequency-agile elements in tunable microwave and millimeter wave devices.

[1]G. Subramanyam, M. W. Cole, N. X. Sun, T. S. Kalkur, N. M. Sbrockey, G. S. Tompa, X. Guo, C. Chen, S. P. Alpay, G. A. Rossetti, K. Dayal, L.-Q. Chen, and D. G. Schlom, J. Appl. Phys. **114**, 191301 (2013).
[2]L. Davis and L. G. Rubin, J. Appl. Phys. **24**, 1194 (1953).
[3]J. Bellotti, E. K. Akdogan, A. Safari, W. Chang, and S. Kirchoefer, Integr. Ferroelectr. **49**, 113 (2002).
[4]Z. Yuan, Y. Lin, J. Weaver, X. Chen, C. L. Chen, G. Subramanyam, J. C. Jiang, and E. I. Meletis, Appl. Phys. Lett. **87**, 152901 (2005).
[5]N. K. Pervez, P. J. Hansen, and R. A. York, Appl. Phys. Lett. **85**, 4451 (2004).
[6]F. A. Miranda, F. W. Van Keuls, R. R. Romanofsky, C. H. Mueller, S. Alterovitz, and G. Subramanyam, Integr. Ferroelectr. **42**, 131 (2002).
[7]N. A. Pertsev, A. K. Tagantsev, and N. Setter, Phys. Rev. B **61**, R825 (2000).
[8]A. K. Tagantsev, V. O. Sherman, K. F. Astafiev, J. Venkatesh, and N. Setter, J. Electroceram. **11**, 5 (2003).
[9]R. J. Cava, J. Mater. Chem. **11**, 54 (2001).
[10]S. S. Gevorgian and E. L. Kollberg, IEEE Trans. Microw. Theory Tech. **49**, 2117 (2001).
[11]L. B. Kong, S. Li, T. S. Zhang, J. W. Zhai, F. Y. C. Boey, and J. Ma, Prog. Mater. Sci. **55**, 840 (2010).
[12]D. Dimos and C. H. Mueller, Annu. Rev. Mater. Sci. **28**, 397 (1998).
[13]D. Dimos, M. V. Raymond, R. W. Schwartz, and H. N. Al-Shareef, J. Electroceram. **1**, 145 (1997).
[14]K. P. Jayadevan and T. Y. Tseng, Mater. Sci. Mater. Electron. **13**, 439 (2002).
[15]M. B. Okatan, A. L. Roytburd, J. V. Mantese, and S. P. Alpay, J. Appl. Phys. **105**, 114106 (2009).
[16]A. L. Roytburd, S. Zhong, and S. P. Alpay, Appl. Phys. Lett. **87**, 092902 (2005).
[17]N. A. Pertsev, P. E. Janolin, J.-M. Kiat, and Y. Uesu, Phys. Rev. B **81**, 144118 (2010).
[18]A. P. Levanyuk and I. B. Misirlioglu, J. Appl. Phys. **110**, 114109 (2011).
[19]M. W. Cole, P. C. Joshi, M. Ervin, M. Wood, and R. L. Pfeffer, J. Appl. Phys. **92**, 3967 (2002).
[20]A. Erbil, Y. Kim, and R. A. Gerhardt, Phys. Rev. Lett. **77**, 1628 (1996).
[21]B. D. Qu, W. L. Zhong, and R. H. Prince, Phys. Rev. B **55**, 11218 (1997).
[22]M. W. Cole, E. Ngo, C. Hubbard, S. G. Hirsch, M. Ivill, W. L. Sarney, J. Zhang, and S. P. Alpay, J. Appl. Phys. **114**, 164107 (2013).
[23]M. Dawber, N. Stucki, C. Lichtensteiger, S. Gariglio, P. Ghosez, and J. M. Triscone, Adv. Mater. **19**, 4153 (2007).
[24]I. B. Misirlioglu, G. Akcay, S. Zhong, and S. P. Alpay, J. Appl. Phys. **101**, 036107 (2007).
[25]H. Wu, A. Liu, L. Wu, and S. Du, Appl. Phys. Lett. **93**, 242909 (2008).
[26]Y. G. Wang, W. L. Zhong, and P. L. Zhang, Phys. Rev. B **51**, 17235 (1995).
[27]N. A. Pertsev, A. G. Zembilgotov, and A. K. Tagantsev, Phys. Rev. Lett. **80**, 1988 (1998).
[28]J. Zhang, M. W. Cole, and S. P. Alpay, J. Appl. Phys. **108**, 054103 (2010).
[29]M. J. Haun, E. Furman, H. A. McKinstry, and L. E. Cross, Ferroelectrics **99**, 27 (1989).
[30]M. T. Kesim, J. Zhang, S. Trolier-McKinstry, J. V. Mantese, R. W. Whatmore, and S. P. Alpay, J. Appl. Phys. **114**, 204101 (2013).
[31]M. G. Harwood, P. Popper, and D. F. Rushman, Nature **160**, 58 (1947).